

Chapter 1

Introduction to silicon trackers at LHC

1.1 Radiation hard silicon trackers for the LHC

Trackers at design luminosity

CERN¹ is presently constructing the Large Hadron Collider (LHC), which will produce collisions of 7 TeV protons in 4 interaction points at a design luminosity² of $10^{34} \text{ cm}^{-2} \text{ s}^{-1}$. Each of the interaction points is equipped with large detectors built by 4 international collaborations³.

Silicon microstrip and pixel sensors are at present the most precise tracking detectors for charged particles in high energy physics experiments. They have an excellent position resolution of a few tens of micrometers, their signal collection time is short, they can be operated in strong magnetic fields and their thickness (of the order of 300 μm) represents only 0.3 % of the radiation length⁴.

The particle trackers immediately around the collision point are exposed each 25 ns to several hundred secondary particles issued from about 20 head-on p-p collisions. Already at the design luminosity, the inner layers of the trackers will have to deal with unprecedented radiation levels. They will receive doses in the range of 200 kGy at 10 cm radius from the collision point in ten years of operation, entailing serious radiation damage of the silicon sensors and their front-end readout electronics.

Figure 1.1 shows the expected fluences after 10 years of LHC at the CMS silicon tracker. The total fluence is shown as a function of radial distance to the interaction point for two z locations along the beam axis, namely 10 cm and 250 cm. The contributions from charged hadrons and neutrons with energies higher than 100 keV are shown by the dotted and dashed lines, respectively, for both z locations. The total fluence ranges between 10^{14} cm^{-2} and 10^{15} cm^{-2} at the inner tracker layers. This fluence can be directly compared to the one expressed in terms of 1 MeV equivalent neutrons, which is the parameter often used to evaluate the damage in silicon detectors.

1 European Laboratory for Particle Physics, Geneva, Switzerland (www.cern.ch).

2 The luminosity L is related to the total event rate R by the total interaction cross section σ_{int} as $L = R/\sigma_{\text{int}}$.

3 ATLAS (A Toroidal LHC Apparatus), CMS (Compact Muon Solenoid), ALICE (A Large Ion Collider Experiment), LHCb (The Large Hadron Collider beauty experiment).

4 The radiation length is the mean distance over which a high-energy electron loses all but 1/e of its energy by bremsstrahlung. For silicon, the radiation length is 21.82 g/cm^2 (9.36 cm).

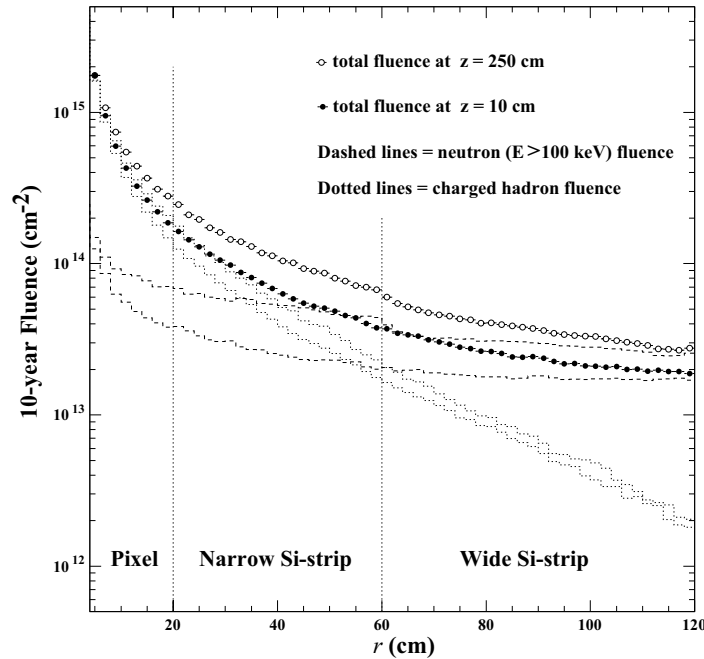


Figure 1.1 Expected fluences at CMS inner tracker after 10 LHC years. Extracted from CMS week plenary session talk, 13th December 2000, Bombay. Courtesy of M. Huhtinen.

Trackers after luminosity upgrade

Studies of the physics potential and experimental challenges of a future high-luminosity ($10^{35} \text{ cm}^{-2} \text{ s}^{-1}$) upgrade of the LHC have been carried out [1]. To reach this luminosity, proton bunches will have to collide with 5 ns to 12.5 ns intervals, yielding 80 to 200 collisions and 480 to 1200 charged tracks, respectively, per interval and per unit of pseudorapidity¹. Such track and vertex densities require a very fine segmentation of the detectors, which increases the number of output channels and therefore the total cost, and puts a high stress on the reduction of the cost per channel. Obviously also the speed of the charge signal and of the electronics are important questions.

A feasibility study for upgrading the LHC has been launched at CERN [2], which develops scenarios for increasing both the luminosity and the beam energy in the two high-luminosity experiments. A staged upgrade of the LHC and its injectors has been considered, compatible with established accelerator design criteria and fundamental limitations of the hardware systems, aiming a target luminosity in proton operation of $10^{35} \text{ cm}^{-2} \text{ s}^{-1}$ in the high-luminosity experiments, and an upgrade of the centre of mass energy to 28 TeV.

In a first phase, the maximum performance without hardware changes to the accelerator would be achieved by colliding beams only at two interaction points, increase the bunch population to $1.7 \cdot 10^{11}$ protons per bunch, and increase the main dipole field to 9 T, resulting in a proton energy of 7.54 TeV. Increasing the LHC luminosity with hardware changes only in the LHC insertions (modification of the quadrupoles layout) and injectors would be a second phase of the upgrade. A third

¹ The pseudorapidity is an angle defined as $\eta = -\ln \tan(\theta/2)$, where $\cos \theta = p_z/p$, p being the 4-momentum and z the beam direction.

phase considers major hardware changes to the LHC such as modification of the injectors to increase significantly the brilliance; equip the Super Proton Synchrotron (SPS) with superconducting magnets in order to inject into the LHC at 1 TeV; or install new superconducting dipoles to reach a beam energy of 14 TeV.

Radiation damage in silicon detectors

The radiation dose resulting from the operation at high luminosity will cause a serious deterioration of the silicon detector performance. The main damage effects are a proportional increase of the leakage current¹ with fluence, an increase of the full-depletion potential and a decrease of the charge collection efficiency.

The operation of the detectors is limited by the maximum potential which can be applied without provoking breakdown. The full-depletion potential rises with increasing dose. If the operating potential is lower than the full-depletion potential, the signal from the undepleted region is lost.

A low bias potential is desirable because it avoids the use of costly design and processing features required for preventing electrical breakdown. The mechanism by which the radiation-induced defects in silicon increase the full-depletion potential can be understood by considering their deep energy levels in the forbidden bandgap of the electronic system in silicon. The initial space charge density in n-type silicon is positive (donor type impurities dominate) and is $\leq 10^{12} \text{ cm}^{-3}$. The acceptor type deep energy levels dominate in radiation-induced defects that lead to the changes in the net effective concentration (N_{eff}) in the detector space charge region. Therefore, at higher fluence Φ (beyond 10^{13} cm^{-2} for neutrons and protons) N_{eff} becomes negative and increases nearly proportional to Φ . This effect is known as type inversion.

The leakage current increases when the detector is irradiated. This effect is strongly temperature dependent and operation at low temperature has the beneficial effect of reducing the leakage current, which is a source of the detector noise, and also of heat generation inside the detector substrate. Therefore, to avoid a strong rise of noise the detector needs to be cooled to about $-10 \text{ }^\circ\text{C}$ when operated in a harsh radiation environment. This also offers the further advantage of a suppressed reverse annealing, which would increase the full-depletion potential even higher.

Last but not least, charge loss by trapping in radiation induced defects is also a key factor in the reduction of signal due to radiation damage at extremely high doses.

Radiation hard silicon detectors after luminosity upgrade

The state-of-art silicon microstrip detectors can tolerate a fluence of about $3 \cdot 10^{14} \text{ cm}^{-2}$ of hadrons or charged leptons. This is insufficient, however, for long-term operation in the central parts of the LHC trackers, in particular after the possible luminosity upgrade of the LHC. The problem of radiation tolerance of these devices becomes extremely severe, because the fluence will be up to 10^{16} cm^{-2} in the inner layers and it has led to intense efforts for the development of radiation hard material.

1 Basic concepts of semiconductor physics are collected in the Appendix.

An approach for improvement of silicon radiation detectors is based on the modification of the properties of silicon by doping with different impurities or lattice defect (material engineering). The studies on oxygenated¹ Float Zone (Fz) and Czochralski (Cz) silicon sensors are mainly coordinated by the CERN RD50 collaboration [4]. It has been found [5] that there is a beneficial effect of a high oxygen concentration on the radiation hardness of silicon detectors. Typically, the full-depletion potential of a 300 μm thick detector fabricated from oxygen enriched and standard Fz silicon after being exposed to a 23 GeV proton fluence of $\phi_{\text{eq}} = 6 \cdot 10^{14} \text{ cm}^{-2}$, is 300 V and 800 V, respectively. However, while the improvement of the radiation hardness is by a factor of 2-3 for protons, no improvement is revealed for neutron-irradiated detectors. Despite the benefits of oxygen in silicon, cooling of the detectors is inevitable in order to reduce the leakage current and suppress reverse annealing, as mentioned above.

Another approach to improve the radiation hardness is that of the CERN RD39 collaboration [6], which develops new detector techniques for trackers which meet the goals set by the requirements of LHC after its luminosity upgrade to $10^{35} \text{ cm}^{-2}\text{s}^{-1}$, based on the operation of the detectors at low temperature. Many advantages arise from the cryogenic operation of the silicon detectors in heavy radiation environment: suppression of the leakage current, low full-depletion potential, fast charge transit (higher carrier drift mobility), charge collection efficiency increase, faster readout electronics and lower noise, improved thermal stability of sensors. Modeling of the effects of deep defects has shown that the electric field in irradiated silicon detectors can be manipulated by changing the filling status of deep defect levels, obtained by injecting a small current of holes at cryogenic temperatures. Further explanation of the behaviour of silicon sensors at low temperature is given in Section 1.2.

1.2 Cryogenic silicon microstrip detector modules for the LHC

The RD39 Collaboration [6] develops new detector techniques for trackers capable of surviving fluences up to 10^{16} cm^{-2} accumulated in the inner layers of the LHC microstrip trackers after its luminosity upgrade. These techniques are based on the operation of silicon sensors at low temperature. The goals of RD39 are therefore to improve the radiation hardness by a factor of 10 or more above the present state-of-art silicon detectors, to develop segmented silicon detectors with faster signal and higher signal to noise ratio, to produce detector modules and to develop low-mass cryogenic systems for experiments in high energy physics.

It was only in 1998 [7] when it was noted for the first time that operation of Si sensors at cryogenic temperatures might improve their radiation hardness, when Palmieri *et al.* observed that the cooling of irradiated silicon diode sensors, biased so that they were underdepleted at room temperature, resulted in a spectacular recovery of their charge collection efficiency, as shown in detail in [8] and in Figure 1.2. However, this improvement is not permanent because of inevitable polarization of the bulk silicon, if the detector is operated in the normal reverse bias mode. This could be avoided by operating in the forward bias mode, which was demonstrated to be possible at low temperatures for detectors irradiated by $10^{15} \text{ n}\cdot\text{cm}^{-2}$. The result suggested that the symmetric structure $\text{p}^+\text{-i}\text{-p}^+$ could also be used after pre-irradiation, which turned out to be a promising technique for the control of the electric field at low temperatures and under heavy irradiation.

1 Silicon with high oxygen concentration obtained by manufacturing process.

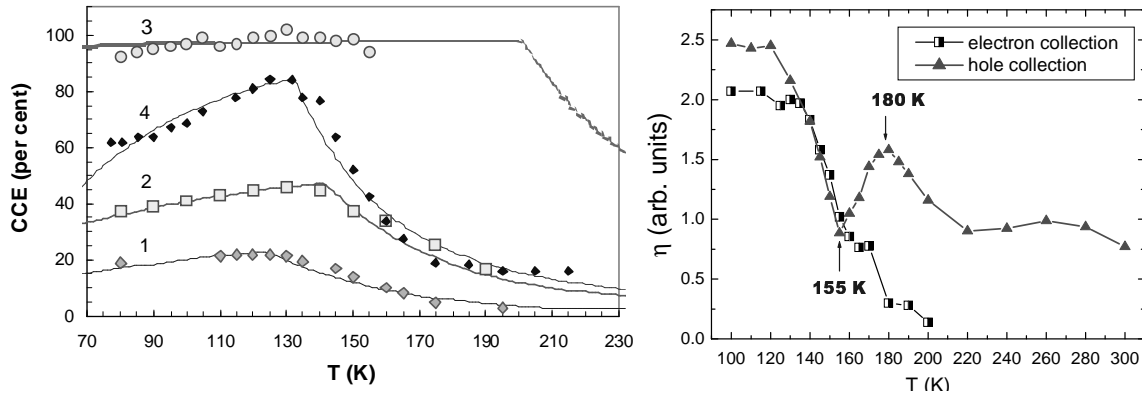


Figure 1.2 On the left: Temperature dependence of the charge collection efficiency for minimum ionising particles (MIPs) traversing detectors irradiated by neutrons. Points - experimental data, solid lines - simulated curves. Neutron fluences (cm^{-2}): 1 - 10^{15} ; 2 - $5 \cdot 10^{14}$; 3, 4 - 10^{14} . Reverse bias potential: 1, 2, 3 - 250 V; 4 - 100 V [8][9]. On the right: Efficiency of electron and hole collection after a pulse of red light in a detector made of Float Zone silicon, irradiated by neutron fluence of $5.15 \cdot 10^{15} \text{ cm}^{-2}$ [10].

The main improvement in radiation hardness, in terms of the increase of charge collection efficiency, is obtained by manipulating the charge state of radiation induced deep-level defects and by changing the properties of radiation induced traps, using such tools as the temperature of the detector and the injection of charge by a forward biased junction or by light.

Recovery of the charge collection efficiency of irradiated silicon at low temperatures

The deterioration of the charge collection efficiency is due to trapping of charge carriers. The particle radiation induces trapping centres that eventually lead to a reduction in the signal height produced by minimum ionising particles (MIPs). The charge collection efficiency η can be considered to be a product of two factors [10]:

$$\eta = \eta_{\text{GF}} \cdot \eta_t = \left(\frac{W}{d}\right)^2 \exp(-t_{\text{dr}}/\tau_t), \quad (1.1)$$

where W is the depletion depth, d the sensor thickness, τ_t the trapping time constant and t_{dr} the carrier drift time. The first term $\eta_{\text{GF}} = \left(\frac{W}{d}\right)^2$ is a geometrical factor which describes the fraction of the detector that is depleted. The second term is the trapping factor that is related to the trapping of carriers by defects. The trapping (τ_t) and detrapping (τ_d) time constants for a trap level are given by:

$$\tau_t = \frac{1}{\sigma v_{\text{th}} N_t}; \quad (1.2)$$

$$\tau_d = \frac{1}{\sigma v_{\text{th}} N_C \exp(-E_t/kT)}, \quad (1.3)$$

where σ is the capture cross section of the trap, v_{th} is the thermal velocity of the charge carriers, N_t is the concentration of traps, N_C the electric state density in the conduction band and E_t the trap energy level in the band gap.

It has been seen that the η_{GF} can be increased close to 1 by current or charge injection at temperatures from 130 K to 180 K. This is described in the next subsection. On the other hand, as shown by Figure 1.3, there is a strong temperature dependence of N_{eff} . The figure shows this dependence for standard Si and oxygenated Si samples irradiated by extremely high doses (~ 17 MGy) of γ rays. For standard Si, $N_{eff}(T)$ shows non-monotonic behavior with space charge sign inversion, which is quite unique for irradiated detectors, and is related with the temperature dependence of the deep level filling. The slight increase in N_{eff} from its initial value of $-6 \cdot 10^{12} \text{ cm}^{-3}$, which occurs from RT to 220 K, is followed by a sharp increase up to about zero and space charge inversion at $T = 200$ K. The maximum positive N_{eff} of $2 \cdot 10^{12} \text{ cm}^{-3}$ is achieved at $T \approx 190$ K after which N_{eff} goes down monotonically to a saturated value of $\sim 3 \cdot 10^{11} \text{ cm}^{-3}$. For oxygenated Si, N_{eff} is positive at any T and at $T < 190$ K N_{eff} has the same positive value in both types of silicon detector, which indicates that the same deep levels contribute to N_{eff} .

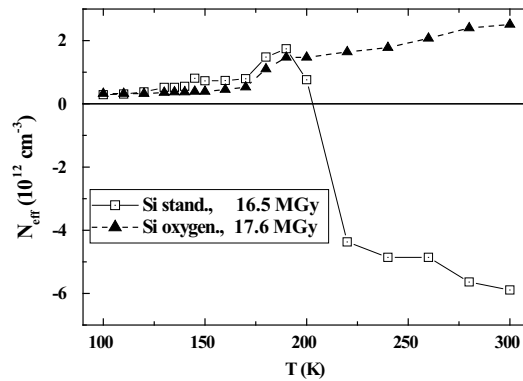


Figure 1.3 $N_{eff}(T)$ for detectors made of standard and oxygenated silicon and irradiated by an ultra-high dose of γ rays [10].

The high full-depletion potential of heavily irradiated silicon detectors is due to various radiation-induced defects. Two deep levels are recognized responsible for the main increase of the effective doping concentration, and adopted as basis of the modeling of radiation effects [9], namely a deep donor $E_v + 0.48$ eV and a deep acceptor $E_c - 0.527$ eV. The capture cross section of both levels is about 10^{-15} cm^2 . It could happen that the trapping time constant would limit the collection of charge carriers within $20 \mu\text{m}$ - $30 \mu\text{m}$ even if the $300 \mu\text{m}$ thick detector would be fully depleted, representing that 80 %-90 % detector volume is not used.

The term η_t becomes important for high fluences ($> 10^{15} \text{ n cm}^{-2}$) (the trapping time constant depends weakly on the temperature but strongly on the radiation fluence). In order to overcome the reduction of η at high fluences, the η_t is modified at low temperatures taking advantage of the temperature dependence of the detrapping time. This dependence makes it possible to freeze out trapping centers at low temperatures. If a trap is filled (by current injection or charge injection) and then frozen at cryogenic temperatures, this trap will no longer be able to trap free carriers again, and it becomes electrically inactive. Then η_t becomes nearly 1 and η can be significantly improved. To freeze out both deep and shallow levels one needs to go to cryogenic temperatures. As an example of the temperature dependence of the detrapping time constant, Table 1.1 shows this constant for the A-center¹ defect [6].

¹ The A-center is a shallow radiation induced trapping center at $E_c - 0.18$ eV with a capture cross section of 10^{-15} cm^2 .

Table 1.1 Temperature dependence of the detrapping time constant for the A-center.

Temperature (K)	τ_d
300	10 ps
150	10 ns
100	10 μ s
77	6 ms
60	12 s
55	5 min
50	3.6 h
45	15 days
40	13 years

Space charge manipulation by current injection

In order to reach low N_{eff} the densities of positively and negatively charged defects must be equal. This can be done by internal electric field manipulation using carrier injection. The injected current density and the applied potential control the electric field profile. This current is very stable, because it is limited by the space charge, and its effect is to stabilize the electric field in the bulk silicon constituting the sensitive volume of the detector. In the space charge limited current (SCLC) mode, the electric field, at any bias and for any concentration of deep traps, is distributed in the entire volume between the contacts, and therefore the detector stays fully depleted irrespective to its irradiation history. The parameters which determine the current flow through the sample are the temperature and the concentration of radiation-induced defects, the bias potential and possibly the amount and distribution of light incident on the detector contacts.

The current injection into the detector's bulk can be achieved by excitation with a proper light source or by electrical excitation from electrical contacts. The latter method is more convenient to put in practice in a high-energy physics experiment. The electrical excitation is done in the symmetric initial p^+n-p^+ structures which are turned into p^+p-p^+ structures after irradiation beyond the space charge sign inversion. Then, one of the $p+p$ contacts injects holes under the applied potential, which then drift in the detector volume. Tests of heavily irradiated forward biased detectors and p^+i-p^+ sensor structures have revealed that the basic idea of the current-injected sensors is sound.

Decrease of the leakage current and edgeless silicon sensors

Thin planar silicon detectors are usually designed so that one side only is patterned, and the sides between the central sensitive area and the cut edges feature one or more guard rings, which permit the minimization of the surface leakage current by confining the superficial electric field on processed high-quality surface with SiO_2 passivation. This technique yields detectors with 0.5 mm to 1.0 mm edges, where the charge signal of normally incident penetrating ionizing particles gradually drops when the particle track moves from the sensitive area towards the edge. For position-sensitive detectors this

results in the loss of tracking accuracy and efficiency in the edge region of 0.5 mm to 1.0 mm width [11].

Edgeless position sensitive detectors are of interest in imaging applications using non-penetrating radiation such as soft X-rays or vacuum ultraviolet, and in applications where the sensor must be positioned as close as possible to a particle beam or to a wall. In the first case the edge sensitivity permits contiguous imaging with overlapped sensors, while in the latter category very forward scattering amplitudes and cross sections can be measured down to very small momentum transfer.

When a structure is cut through its contact implants, a large surface current on such an edge prevents the normal reverse biasing of the device at full-depletion potential. However, the current can be sufficiently reduced by the use of a suitable cutting method, followed by edge treatment and by operating the sensor at low temperature. The edge sensitivity of an edgeless diode and microstrip sensor have been studied with a high energy beam. All these results are reported in Chapter 6.

Other side benefits of operation at low temperature

Low temperature operation yields important side benefits. At lowered temperature the carrier mobility increases, entailing higher current signal speed and height. The leakage currents are strongly reduced, which eliminates the noise due to the sensor current. The combination of these, together with the lower noise of CMOS readout circuits at low temperature, yield both faster signals and higher signal-to-noise ratio. The bandwidth and switching speed of CMOS circuits are increased at low temperatures, offering a method to increase the readout speed.

From a thermo-mechanical point of view, the thermal conductivity of silicon increases, helping to use less additional heat spreader material, thus reducing the thickness of the detector modules. Moreover, low-temperature detectors can be processed using simpler design with fewer masks, which contribute to the cost reduction and yield increase.

Other benefits follow from the cryogenic vacuum environment. From a thermal point of view, working under vacuum reduces the heat leaks due to convection. Moreover, it avoids the corona discharge of the metallic parts at the high bias potential. The good vacuum leads to a very small thickness of the adsorbed gas layer on the sensors, and thus reduces surface leakage currents. The metallic vacuum chamber shields the detectors from water and other condensible gases, and it also provides a Faraday cage for the tracker.

1.3 LHC luminosity measurement

The development of edgeless silicon microstrip detector modules operated at cryogenic temperatures was initially motivated by the measurement of the very forward elastic scattering at the CERN LHC, needed in the luminosity-independent measurement of the total cross-section.

The TOTEM¹ experiment [12][13] will measure the total cross-section using the luminosity independent method, based on the optical theorem together with a measurement of the total elastic and

1 Total Cross Section, Elastic Scattering and Diffraction Dissociation at the LHC.

inelastic rate to extract an absolute value of the luminosity, as well as the total cross section σ_{tot} . The luminosity L can be expressed as:

$$L = \frac{(1 + \rho^2)}{16\pi} \cdot \frac{(N_{\text{inel}} + N_{\text{el}})^2}{\left. \frac{dN_{\text{el}}}{dt} \right|_{t=0}}, \quad (1.4)$$

where ρ is the ratio of the real to the imaginary parts of the forward amplitude, N_{inel} and N_{el} are the inelastic and elastic pp interaction rates, t is the 4-momentum transfer. This requires the simultaneous measurement of the elastic pp scattering down to the four-momentum transfer of $-t = 10^{-3} \text{ GeV}^2/c^2$ and of the inelastic pp interaction rate with an adequate acceptance in the forward region. The forward differential cross section at $t = 0$ has to be extrapolated from the measurement of the elastic scattering at low momentum transfers. This can be related using the optical theorem, with the event rates due to the elastic and the total cross sections, by:

$$\left. \frac{d\sigma_{\text{el}}}{dt} \right|_{t=0} = \frac{1}{L} \left. \frac{dN_{\text{el}}}{dt} \right|_{t=0} = (1 + \rho^2) \cdot \frac{\sigma_{\text{tot}}^2}{16\pi}, \quad (1.5)$$

where σ_{el} is the elastic cross section and σ_{tot} is the total cross section. From these equations, the total cross section can be calculated independently of the luminosity with the expression:

$$\sigma_{\text{tot}} = \frac{(N_{\text{inel}} + N_{\text{el}})}{L} = \frac{16\pi}{(1 + \rho^2)} \cdot \frac{\left. \frac{dN_{\text{el}}}{dt} \right|_{t=0}}{(N_{\text{inel}} + N_{\text{el}})}. \quad (1.6)$$

In order to measure the inelastic pp interaction (N_{inel}), two tracking telescopes, integrated within the CMS experiment detectors, will be installed on each side of the interaction point. The elastic scattering (N_{el}) will be measured with two sets of detectors sitting in Roman Pots, located symmetrically on each side of the interaction point at 147 m and 220 m (Figure 1.4). At these locations, two Roman Pot stations separated by a distance of 4 m will permit a precise determination of the angle of elastic scattered protons.

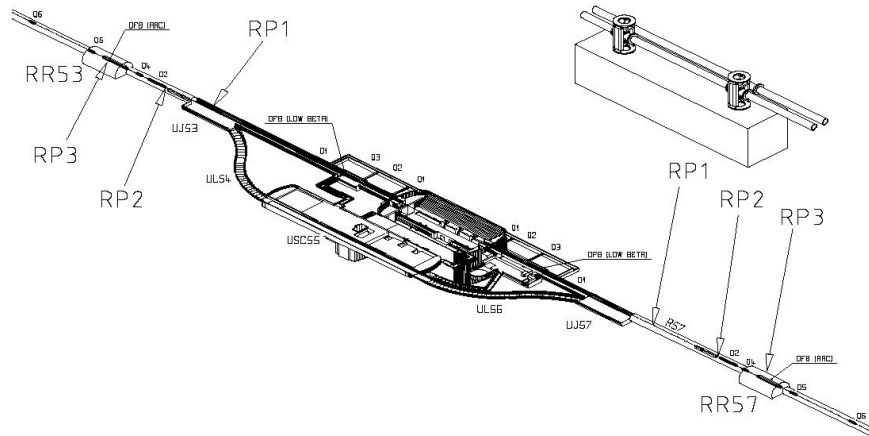


Figure 1.4 The Roman Pot stations will be located on each side of the interaction point at 147 m (RP1) and 220 m (RP3) on the LHC tunnel. A third station (RP2) at about 180 m from the interaction point might be equipped at a later stage.

The accuracy of the experimental total cross section depends critically on the minimum momentum transfer which can be measured, because the functional form of the extrapolation is not known from theory. The beams at the LHC are rather small, with a 10σ envelope of less than 1 mm. The amount of dead space at the edge of detector, i.e. the size of the insensitive region, is therefore a critical parameter. Besides, outside the dead space, the detector has to be close to 100 % efficient with little variation of the efficiency as a function of position. In addition to the dead space of the detector, one also has to consider the thickness of the metallic window that separates the detector from the ultrahigh vacuum of the machine and provides RF isolation, as shown by Figure 1.5.

Using cryogenic silicon detectors for this application has a two-fold benefit. On the one hand, the suppression of the leakage current at low temperatures allows to have edgeless detectors which are sensitive up to their physical edge (Chapter 6). On the other hand, at low temperature there is a radiation hardness improvement, which may be needed for the measurement of luminosity after prolonged exposition of the Roman Pots to full luminosity.

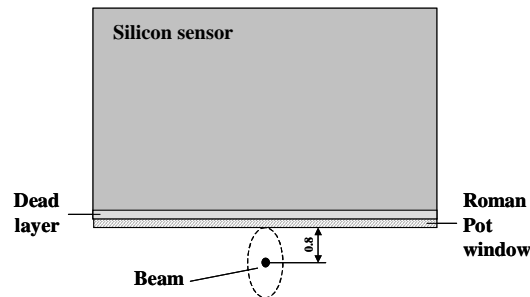


Figure 1.5 The silicon detectors need to be as close as possible to the beam, without interfering with the primary vacuum of the LHC machine. The section shown in the picture points out the importance of using an edgeless silicon sensor, with zero dead layer. Units expressed in mm.

Calculations by N. Mokhov [13] give accumulated dose levels up to 10^5 - 10^6 Gy/yr close to the beam (215 m away from the interaction point and at a distance of 15σ) and at a luminosity of 10^{34} $\text{cm}^{-2}\text{s}^{-1}$. Scaling down to a luminosity of 10^{28} $\text{cm}^{-2}\text{s}^{-1}$, at which the scattering experiment would be performed, gives accumulated doses of 0.1-1 Gy/yr. Here one should further note that a realistic running scenario for elastic scattering is of the order of a week. There is also a contribution to the radiation from the beam halo. Adding the two different contributions, radiation hardness at the level of 100 Gy is sufficient for a dedicated elastic scattering experiment at low luminosity.

1.4 This work

This work proposes a cryogenic module concept which has the features required for the microstrip trackers of the upgraded LHC experiments at CERN. The module can also hold an edgeless sensor, being a good candidate for improved luminosity and total cross-section measurements in the ATLAS, CMS and TOTEM experiments.

The thermal and thermoelastic design of cryogenic silicon microstrip detector modules is described in Chapter 2, with emphasis in the component materials, the cooling and alignment aspects. The thermoelastic properties of the epoxies used to assemble a module being a key factor on the design, Chapter 3 presents a series of measurements carried out at CERN of the thermoelastic properties of

radiation hard epoxies. In order to validate the main design principles, thermal tests were carried out on a mechanical module (Chapter 4). Once the design had been completed and tested from a thermoelastic point of view, a module with real components was assembled. In Chapter 5, first results from the electronics characterization at low temperature are shown. Finally, measurements in a high-energy beam of the edge sensitivity of edgeless silicon pad diode sensors are presented in Chapter 6.

